Polymer 51 (2010) 2652–2660

Contents lists available at ScienceDirect

Polymer

journal homepage: www.elsevier.com/locate/polymer

# Thermal and mechanical properties of poly(3-hydroxybutyrate-*co*-3-hydroxyvalerate)/cellulose nanowhiskers composites

Elena Ten [a], Joel Turtle [a], David Bahr [b], Long Jiang [a,*], Michael Wolcott [a,**]

[a] Composite Materials and Engineering Center, Washington State University, Pullman, WA 99164-1806, USA
[b] School of Mechanical and Materials Engineering, Washington State University, Pullman, WA 99164-2920, USA

ARTICLE INFO

*Article history:*
Received 10 December 2009
Received in revised form
31 March 2010
Accepted 3 April 2010
Available online 14 April 2010

*Keywords:*
Nanocomposite
Cellulose nanowhiskers
Poly(3-hydroxybutyrate-*co*-3-hydroxyvalerate)

ABSTRACT

Bacterial polyester poly(3-hydroxybutyrate-*co*-3-hydroxyvalerate) (PHBV) was reinforced with cellulose nanowhiskers (CNW) in 1–5 wt.% concentrations using a solvent casting method. The CNW was prepared from microcrystalline cellulose (MCC) using sulfuric acid hydrolysis. The influence of CNW on the PHBV crystallization, thermal, dynamic mechanical and mechanical properties were evaluated using polarized optical microscope (POM), differential scanning calorimeter (DSC), dynamic mechanical analysis (DMA), tensile and bulge tests, respectively. POM test results demonstrated that CNW was an effective PHBV nucleation agent. Tensile strength, Young's modulus and toughness of PHBV increased with the increasing concentration of CNW. DMA results showed an increased tan δ peak temperature and broadened transition peak, indicating restrained PHBV molecular mobility in the vicinity of the CNW surface. Storage modulus of the PHBV also increased with the addition of CNW, especially at the temperatures higher than the PHBV glass transition temperature. These results indicated that the CNW could substantially increase the mechanical properties of PHBV and this increase could be attributed to the strong interactions between these two phases.



## 1. Introduction

Due to the growing environmental awareness and concerns over reliable availability of petrochemicals in the future, the polymer industry and academia have been pressed to design and produce polymers and composites based on renewable natural resources. In the past decades, several biodegradable polymers such as polylactic acid (PLA) and polyhydroxyalkanoates (PHAs) have been developed from renewable substances. Poly(3-hydroxybuterate) (P3HB) is a representative polymer from PHA family, which includes a series of aliphatic polyesters produced by bacteria as carbon and energy storage through natural biosynthesis [1]. PHAs have received a great deal of research interests because their mechanical performance is similar to petroleum-based polymers such as polypropylene [2]. However, P3HB differs in several unsatisfactory manners such as increased brittleness [3] and low thermal stability [4]. The toughness of P3HB is significantly improved by forming the copolymer of hydroxybuterate and hydroxyvalerate (HV) – PHBV, which exhibits lower crystallinity due to the incorporation of HV [5]. Finally, increase in HV content decreases the melting point of PHBV thereby lowering processing temperature and the potential of thermal degradation [6].

Reinforcing fibers of various sizes and forms, e.g., natural plant fiber (cellulose fiber), glass fiber, carbon fiber, carbon nanotubes, etc., have been effectively used in polymer composites as reinforcing agents. Nanofillers, however, are found to be preferential in many applications due to their high surface area, lower concentrations needed to achieve reinforcing effect, and the ability to improve toughness along with strength and stiffness. Cellulose nanowhiskers (CNW) is a biologically derived nano-fiber reinforcement for polymer materials. CNW are needle-like elementary crystallites which occur naturally in the cell walls of many plants and some animals (e.g. tunicin). CNW exhibit a typical length and diameter of 200–400 nm and <10 nm, respectively [7]. CNW has a high surface area and high Young's modulus (ca. 143 GPa) [8], which makes it a suitable candidate for polymer reinforcement.

CNW have been used to reinforce both non-biodegradable and biodegradable polymers. Examples of the non-biodegradable polymers include poly(oxyethylene) [9], poly(vinyl chloride) [10], polyvinyl acetate (PVA) [11], polypropylene [12,13], poly(styrene-co-butyl acrylate) latex [14,15] and waterborne epoxy [16,17]. In general, the resulting composites exhibit improved mechanical properties with the addition of CNW. Surface modification of CNW

* Corresponding author. Tel.: +1 (509) 335 6362; fax: +1 (509) 335 5077.
** Corresponding author. Tel.: +1 (509) 335 6392; fax: +1 (509) 335 5077.
*E-mail addresses:* jianglong@wsu.edu (L. Jiang), wolcott@wsu.edu (M. Wolcott).

0032-3861/$ – see front matter © 2010 Elsevier Ltd. All rights reserved.
doi:10.1016/j.polymer.2010.04.007

is found to play an important role in the properties of the CNW reinforced composites [12,13]. Moreover, the processing methods of the composites, e.g., solution blending vs. melt blending, is also shown to have a strong effect on the properties of the final products [9,15].

The biodegradable polymers used as the matrix for CNW reinforcement included polycaprolactone-based waterborne polyurethane [18], polycaprolactone (PCL) [19], poly(hydroxyalkanoates) (PHA) [20], starch [21–24], cellulose [25], soy protein isolate (SPI) [26], poly(lactic acid) [27–29], cellulose acetate butyrate (CAB) [30–32], and poly(ethylene glycol) [33]. In these studies, CNW was shown to have varying degree of reinforcing effect on the different polymer matrixes.

Most recently Braun et al. reported a single-step isolation and surface functionalization method for CNW [34]. Fischer esterification of hydroxyl groups and the hydrolysis of amorphous cellulose chains occurred simultaneously during the isolation process. FTIR results revealed that about half of the surface hydroxyl groups were esterified using this procedure. Using solvent exchange sol-gel process, Capadona et al. prepared the nanocomposites containing ethylene oxide/epichlorohydrin copolymer and nanowhisker through a template approach [35]. These composites exhibited significantly higher shear storage modulus than did the composites produced by solvent casting. For example, at 25 vol% CNW concentration the shear modulus was 18 and 39 MPa for solution cast and template-made composites, respectively. Moreover, the properties of the template-made nanocomposites followed the prediction of percolation model. Rusli and Eichhorn [36] were able to determine stiffness and deformation of epoxy/CNW nanocomposites under tension and compression stresses using Raman spectroscopy. By measuring molecular deformation corresponding to a shift in the carbonyl (C–O) stretch of cellulose backbone, it was possible to evaluate stress transfer from the compliant matrix to the reinforcing cellulose whiskers.

The effects of CNW on the properties of PHBV were first reported by us in an article where the PHBV/CNW nanocomposites prepared by solution casting and melt blending were compared [37]. No other studies have been reported on this composite system. In this paper, we further elucidate the morphology, crystallization behavior and mechanical properties of the system in an attempt to develop a more complete understanding of this bio-composite system.

Therefore, the objectives for out study were to fabricate PHBV/CNW composites by solution casting method and evaluate their thermal, mechanical and dynamic mechanical properties.

## 2. Experimental section

### 2.1. Materials

PHBV containing 12 mol-% hydroxyvalerate (HV) monomer was supplied by Metabolix Inc, (Cambridge, MA). Organic solvent *N*, *N*-dimethylformamide (DMF) was obtained from Acros Organics (Atlanta, GA). Microcrystalline cellulose (MCC) was provided by Avicel (Type pH-102) and was the raw material for producing the CNW. Sulfuric acid (96% concentration) and polyethylene glycol (PEG) with average molecular weight $M_w$ of 20,000 were purchased from J.T. Baker. Boron nitride was used as a nucleating agent and obtained from Saint-Gobain Ceramics (Louisville, KY).

### 2.2. CNW preparation

Acid hydrolysis of MCC was performed in 64 wt.% sulfuric acid at 44 °C with strong mechanical stirring for 2 h. The produced suspension was diluted 10 times with deionized water and kept in a refrigerator to prevent further reaction. The acid was removed by repeated centrifuge (Sorvall) at 5000 rpm for 5-min for each run until the supernatant was turbid. The supernatant was collected and dialyzed (dialysis tube from Spectrum Laboratories Inc., molecular weight cutoff 12,000–14,000) against deionized water for 4–5 days to remove remaining acid. The dialysis tube was then placed in aqueous PEG solution to concentrate the CNW suspension through osmotic pressure. The CNW suspension was gel-like after the concentration process and it was finally freeze-dried (Labconco FreeZone 4.5) into CNW powder.

### 2.3. PHBV/CNW nanocomposites preparation

5 wt.% PHBV was dissolved in DMF at 80 °C. CNW powder at the concentrations of 1–5 wt.% of solid PHBV was added into the PHBV solution and sonicated in an ultrasonic bath (Branson 1510) for 1 h. Following the sonication, the solution was immediately casted onto a clean glass substrate and evaporated overnight at 50 °C. The molecular weight $M_w$ determined by GPC (GPC Max VE2001, Viscotek) showed that the reduction of $M_w$ due to sonication was ca. 17%. The thickness of the cast films was measured to be 15–30 microns. All the films appeared transparent. To ensure constant moisture and residual solvent contents, all films were conditioned in a desiccator containing calcium sulfate (Drierite) at room temperature for at least 2 weeks prior to any test. Residual solvent content was determined to be less than 2 wt.% after the two-week equilibrium by using a vacuum oven drying method.

### 2.4. Characterization

#### 2.4.1. Transmission electron microscopy (TEM)

The shape and size of CNW were studied by a TEM (JEOL 1200 EX) operating at 100 kV. A drop of CNW water solution was introduced on a formvar and carbon-coated copper grid and the water was evaporated naturally. TEM images of CNW were acquired without any sample staining. To study the morphology of the composite film, a small piece of PHBV/5% CNW film was embedded in acrylic resin (London Resin Company Ltd.) and cured at elevated temperature overnight. Thin sections were cut from the resin with a diamond knife on a Reichert-Jung ultramicrotome. The sections were placed on carbon-coated copper grids and then stained with 2% uranyl acetate for 30 min.

#### 2.4.2. Atomic force microscopy (AFM)

Surface morphology of PHBV/CNW nanocomposite film was investigated by an AFM. The tests were conducted in tapping mode using a Veeco Multimode AFM equipped with a NanoScope IIIa controller (Digital Instruments Inc.). Film surfaces were scanned in air using Si tips (Digital Instruments Inc.) with a resonance frequency of ca. 330 kHz. The scan rate was 0.5 Hz. CNW suspension in water was also used for AFM study to have a better view of CNW. To do this, a drop of each suspension was deposited on freshly cleaved mica surfaces. The solution was completely dried by evaporation at ambient condition before being scanned by AFM.

#### 2.4.3. Thermogravimetric analysis (TGA)

TGA was conducted on a Mettler-Toledo TGA/SDTA851e to determine the thermal stability of the prepared samples. Based on the weight loss of each sample component, a sample composition was estimated for CNW powder and PHBV/CNW films. Approximately 5–10 mg of material was placed in an aluminum pan. After equilibrating at 25 °C for 5 min, the sample was heated to 600 °C at 10 °C/minute under 20 ml/min $N_2$ flow. Three replicates were tested for each sample.

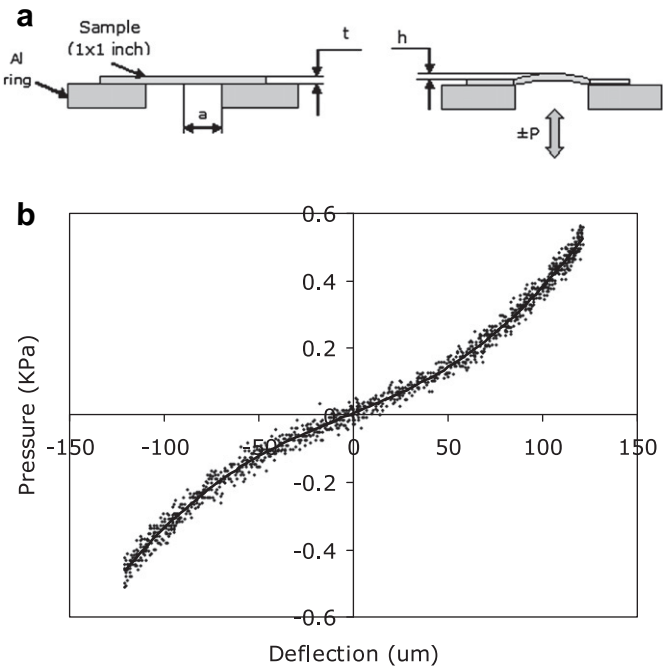


**Fig. 1.** (a) Schematic representation of the bulge test set up; (b) a typical pressure vs. deflection curve of the nanocomposite films obtained from bulge test.

*2.4.4. Polarized optical microscopy (POM)*

Crystallization process of PHBV and PHBV/CNW nanocomposites was studied by Olympus BX51 POM equipped with a Linkam hot stage (THMS600/HFS91). PHBV/CNW films were heated up to 220 °C between two glass slides and then equilibrated at this temperature for 10-min to eliminate any residual PHBV crystallization seeds [38]. The films were then quenched in liquid nitrogen to obtain complete amorphous samples. PHBV nucleation and spherulites growth at 30 °C was examined by the POM and recorded by an attached digital camera after 5 and 20 min of PHBV crystallization.

*2.4.5. Differential scanning calorimetry (DSC)*

Thermal transitions of the nanocomposites were examined by a Mettler Toledo DSC 822e under $N_2$ flow (80 ml/min) and liquid nitrogen controlled cooling. Samples were crimple-sealed in aluminum crucibles and heated from −50 to 200 °C at a heating rate of 10 °C/min (first heating scan), equilibrated at 200 °C for 2 min, cooled rapidly at 30 °C/min to −50 °C, equilibrated at −50 °C for 2 min, and heated up again to 200 °C at 10 °C/min (second heating scan). The first and second heating scans examined the thermal behaviors of the samples with and without previous thermal history, respectively.

*2.4.6. Dynamic mechanical analysis (DMA)*

DMA was conducted in tension mode on a Tritec 2000 DMA at 1 Hz to examine thermal dynamic properties of the films. DMA samples (10 × 6.5 $mm^2$) were cut from the cast PHBV/CNW composite film. Dynamic strain sweep was first performed to determine linear viscoelastic range of the samples. Then the samples were tested from −40 °C to +80 °C at 5 °C/min with a displacement of 0.001 mm. Five replicates were tested for each sample.

*2.4.7. Tensile test*

Dumbbell-shaped film specimens were prepared with a Type IV (ASTM D638) sample cutter and tested according to ASTM D 638–91. Ten samples for each formulation were tested using an Instron 4466 (capacity 500 N) at a tensile rate of 5 mm/min. Tensile strain were monitored by an EIR laser extensometer (model LE-05).

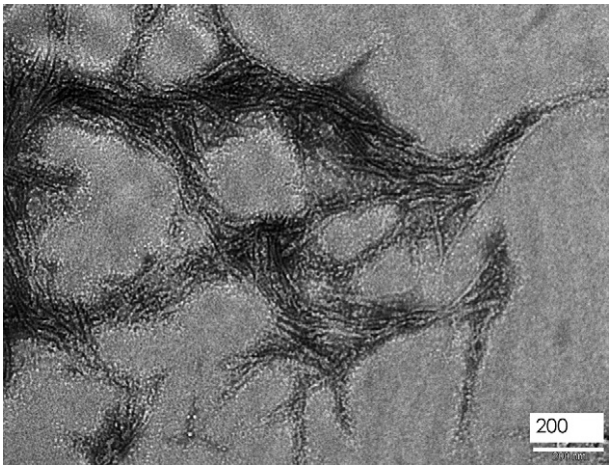


**Fig. 2.** TEM micrograph of CNW. The sample was obtained by evaporating CNW water solution (ca. 2.7 × $10^{-6}$ wt.%) on a formvar-coated copper grid.

*2.4.8. Bulge test*

The bulge test is a standard technique to characterize mechanical properties of thin films, such as residual stresses and elastic modulus. In bulge testing the composite films were wax-mounted onto an aluminum substrate with a pre-drilled hole (Fig. 1a). A varying gas pressure was applied to the film through the hole using a Meriam pressure/vaccuum variator and the resulting film deflection was monitored with a scanning laser vibrometer (Polytec OFV500). The pressure and deflection values were acquired using LabView software. Five replicates were tested for each specimen. By fitting the curve of pressure versus deflection to a cubic polynomial, Young's modulus of the film could be calculated from the slope of the polynomial using the model of circular membrane behavior under uniform pressure [39]:

$$P = \frac{8Et}{3a^4}h^3 + \frac{4t\sigma}{a^2}h$$

where $P$ is gas pressure, $E$ is sample modulus, $t$ is sample thickness, $a$ is bulge radius (4.7625 mm), $h$ is the deflection and $\sigma$ is the residual stress in the film determined by $Pa^2/(4ht)$. Fig. 1b presented a typical set of pressure vs. deflection data of a PHBV/CNW film and its cubic polynomial fitting. The outstanding fitting demonstrated that the film followed the circular membrane behavior depicted by the model.

## 3. Results and discussions

### 3.1. Morphology of CNW and the composite film

The morphology and dispersion of CNW in water was observed using TEM (Fig. 2). Although the whiskers agglomerated on the copper grid after water evaporation, individual whiskers can still be clearly distinguished. The diameter of the whiskers was estimated to be 20 nm. The length of the whisker was difficult to determine due to the whisker agglomeration. However, the AFM images of CNW showed that the whiskers had a wide distribution in fiber length, ranging from 50 nm to 500 nm (Fig. 3). The diameters of CNW obtained from both TEM and AFM were similar. It has been reported that CNW diameter is often overestimated from AFM

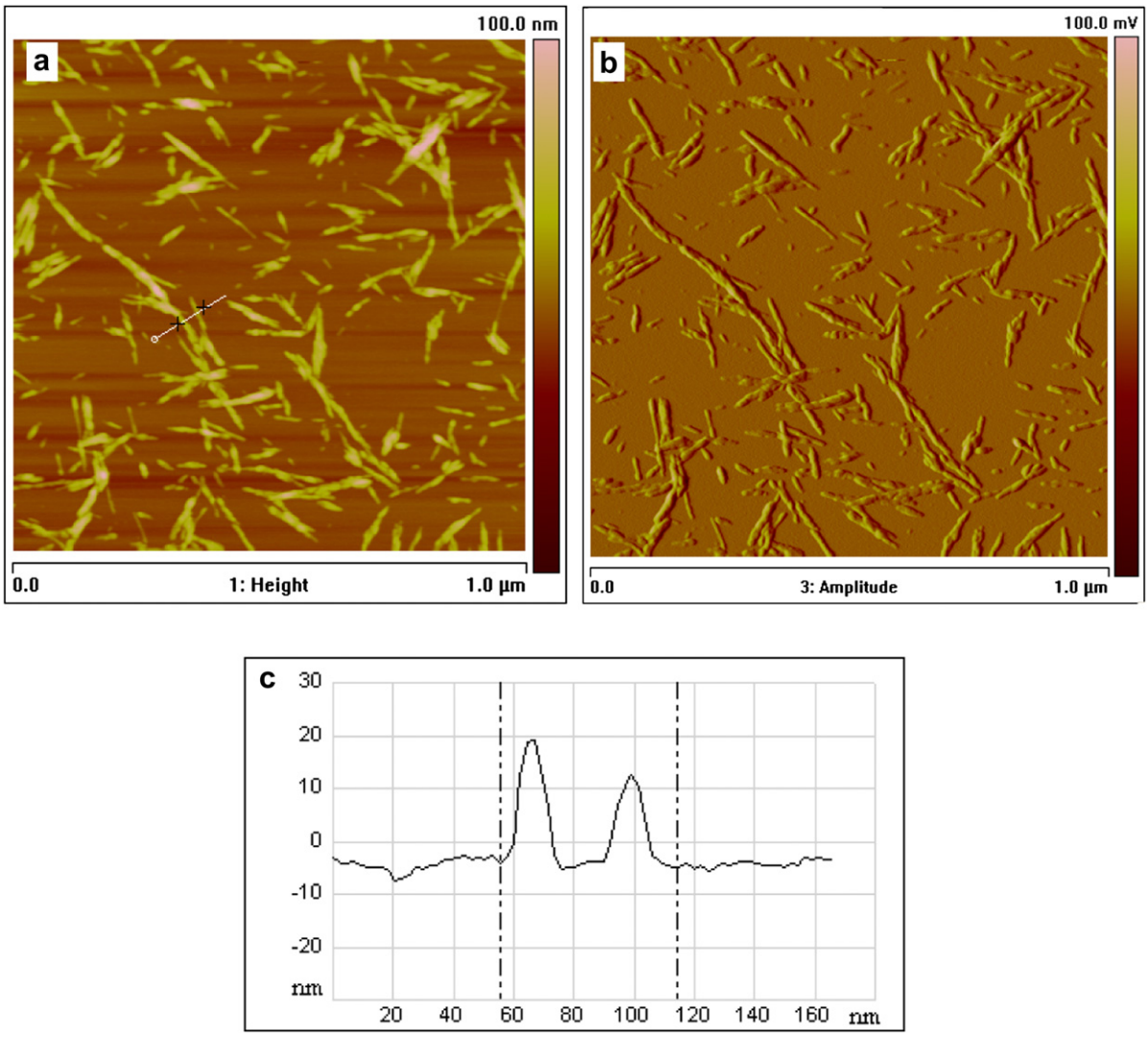


**Fig. 3.** AFM images of CNW. The sample was obtained by evaporating CNW water solution (ca. $2.7 \times 10^{-6}$ wt.%) on a freshly cleaved mica surface. (a) topography, (b) phase image, (c) height profile of the selected line in figure (a).

images due to the tip broadening effect [40]. This effect occurs when the size of the scanning tip is comparable to that of the sample and it enlarges the lateral sizes of the sample artificially due to the cone shape of the tip. In this study, AFM height profiles (which were free of this artifact) rather than AFM images were used to determine the CNW diameter (Fig. 3c). Therefore the diameter values obtained from both TEM and AFM were similar.

TEM micrographs of the PHBV/CNW composite demonstrated a homogenuous dispersion of CNW in the PHBV matrix (Fig. 4). AFM examination confirmed this dispersion state (Fig. 5).

### 3.2. Thermal and mechanical characterization

Thermal degradation of the neat PHBV, CNW powder, and the PHBV/CNW composite were studied by TGA (Fig. 6). It was found that the CNW powder decomposed through a two stage weight loss process, with the first weight loss peak occurring at ca. 307 °C and the second one at ca. 410 °C. Comparing the trace of CNW powder to that of the neat PEG, the first and the second stage could therefore be attributed to the decomposition of CNW and PEG, respectively. The occurrence of PEG in the CNW powder is likely to have resulted from the penetration of the low molecular weight PEG during dialysis. During CNW powder preparation, PEG solution was used to concentrate CNW solution through osmosis. Although the dialysis tube had a molecular weight cutoff of 12,000–14,000 and the PEG used had a weight average molecular weight ($M_w$) of

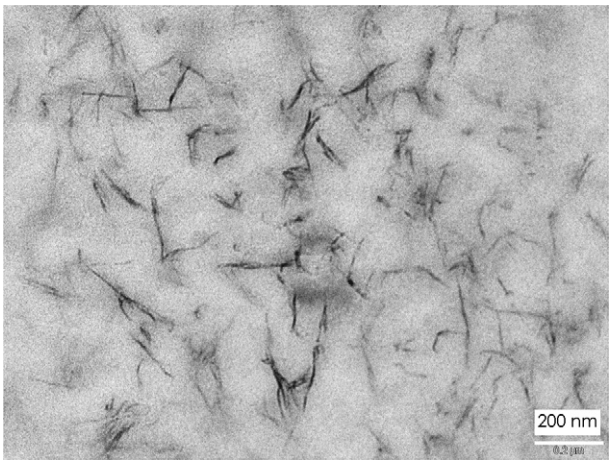


**Fig. 4.** TEM images of the PHBV/5% CNW nanocomposite film at 75 k magnification.

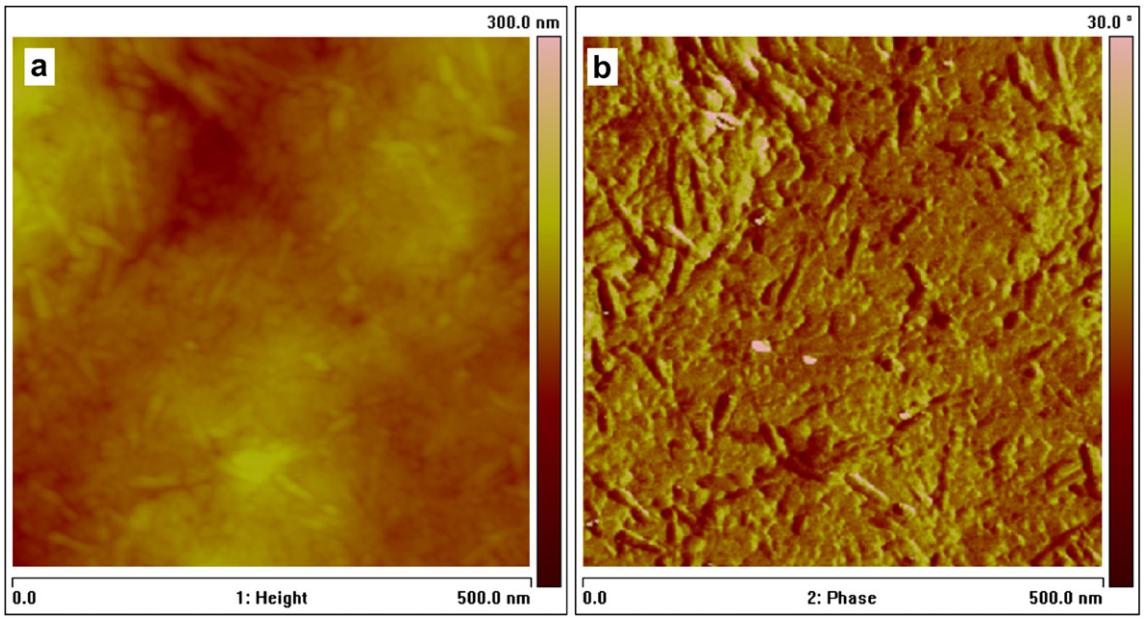


**Fig. 5.** AFM images of PHBV/5% CNW composite film. (a) topography, (b) phase image.

20,000, it was obvious that some low molecular weight PEG still penetrated the tube and mixed with CNW. Based on the weight losses of the two stages, the contents of CNW and PEG in the CNW powder were calculated to be ca. 61 and 30 wt.%, respectively. The remaining ca. 9 wt.% residual could be salts and other inorganic compounds produced from the acid hydrolysis reaction. It is worth noting that the hydroxyl groups of PEG can hydrogen bond with the hydroxyl groups of CNW. PEG was also miscible with PHBV in molten and solution states [41]. Therefore, the PEG in the CNW powder was expected to increase the compatibility between CNW and the PHBV matrix in the composite film.

Comparing the TGA curves of the neat PHBV and the PHBV/5% CNW composite, the addition of CNW was found to slightly reduce the decomposition (maximum weight loss rate) temperature (from ca. 295–290 °C) of the polymer matrix. This phenomenon has been reported in other cellulose nanocrystal reinforced composites [42]. The reason was believed to be due to the increased thermal conductivity of the sample after the addition of CNW [43].

To evaluate the effects of CNW on the thermal behavior of the composites, DSC traces of the PHBV/CNW composites and the neat PHBV were compared (Fig. 7a,b). The second heating scan often

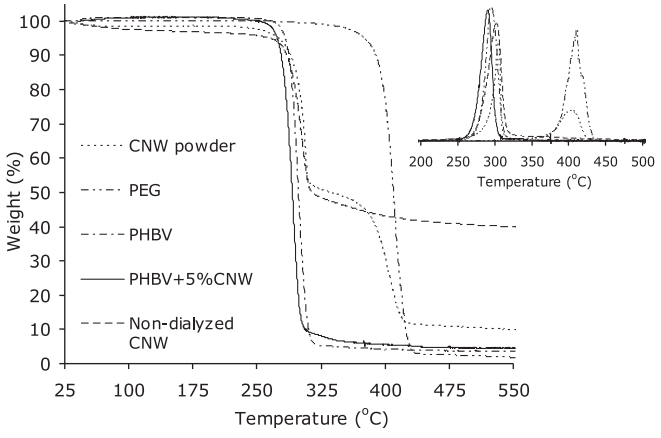


**Fig. 6.** TGA traces of the neat PHBV, neat PEG, CNW powder (dialyzed and non-dialyzed), and the PHBV/CNW composite. The inset shows the first derivative of the weight loss.

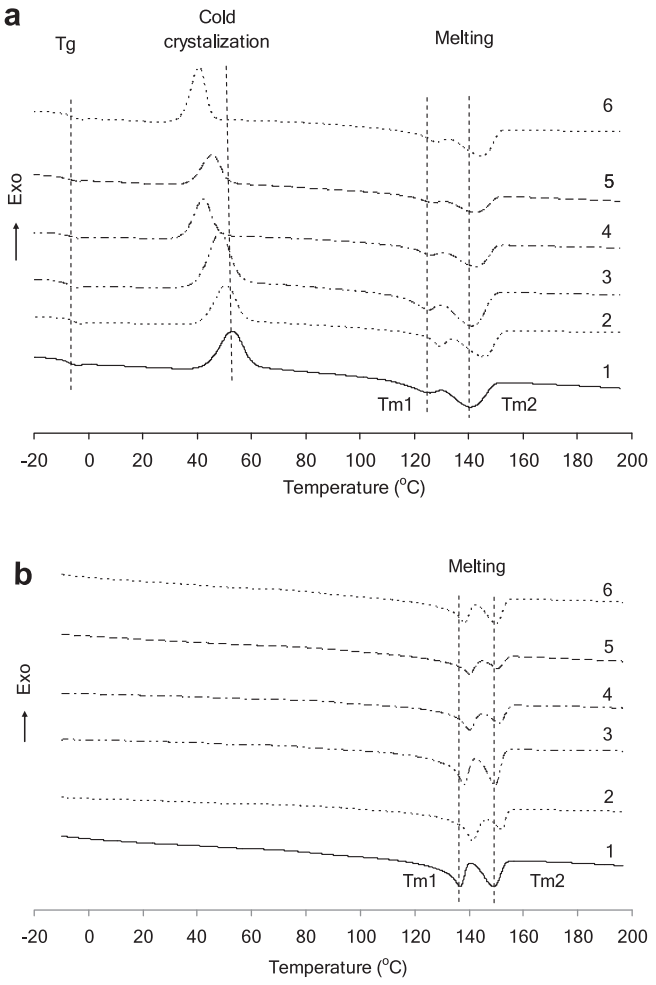


**Fig. 7.** DSC thermograms of neat PHBV and PHBV/CNW nanocomposites from the second (a) and first (b) heating scans. 1, neat PHBV; 2, PHBV+1%CNW, 3, PHBV+2% CNW, 4, PHBV+3%CNW, 5, PHBV+4%CNW, 6, PHBV+5%CNW.

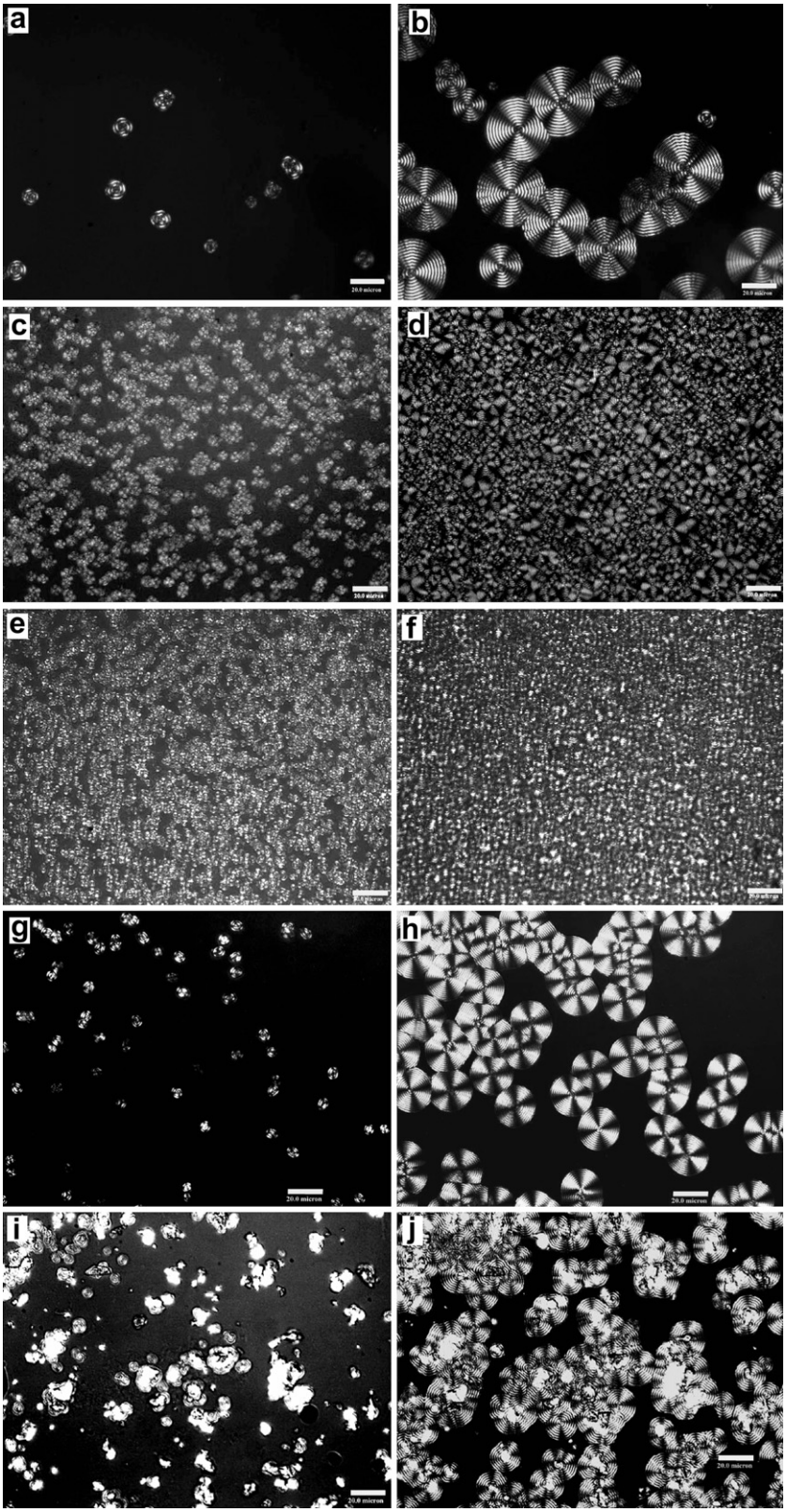


**Fig. 8.** POM micrographs of isothermal crystallization of neat PHBV and PHBV composites at 30 °C. (a) and (b) Neat PHBV, (c) and (d) PHBV/1 wt.% CNW (e) and (f), PHBV/5 wt.% CNW, (g) and (h), PHBV/2 wt.% PEG, (i) and (j) PHBV/1 wt.% boron nitride. Crystallization time: a,c,e,g,i – 5 min; b,d,f,h,j – 20 min. Scale bar represents 20 μm.

reveals more thermal transitions in the material than the first heating scan since most of the thermal and stress histories, which usually cover/weaken thermal transition signals, are erased during the first heating scan. In Fig. 7a (second heating scan), the glass transition, cold crystallization, and melting of PHBV can be clearly seen. The glass transition temperature ($T_g$) of PHBV was not noticeably affected by the addition of various contents of CNW powder. Similar results had been reported in several other studies

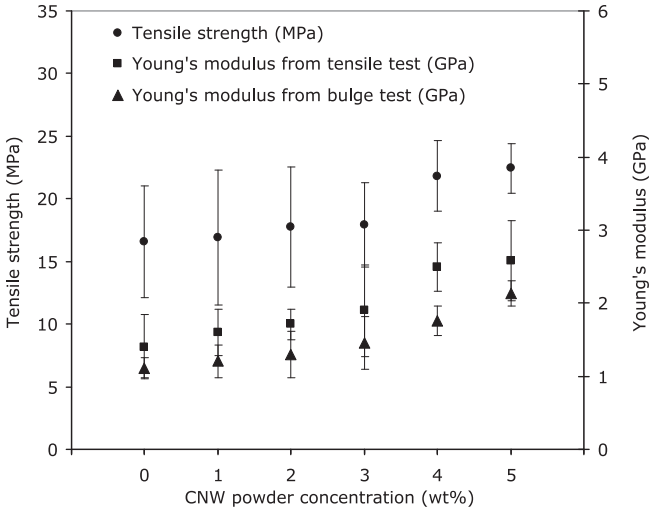


**Fig. 9.** Young's modulus and tensile strength of neat PHBV and PHBV/CNW nanocomposites determined by tensile and bulge tests.

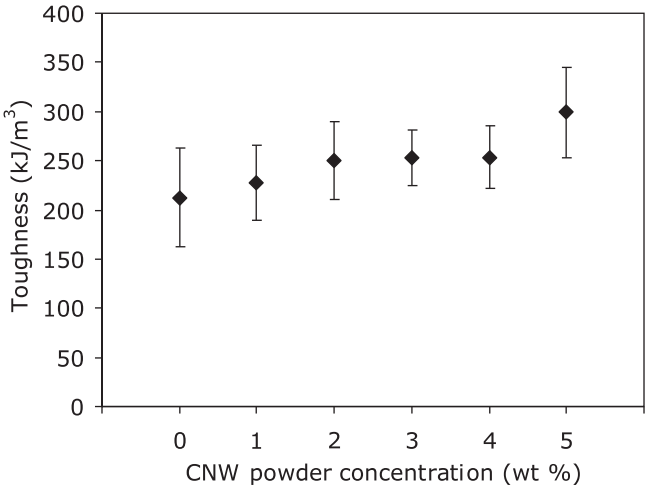


**Fig. 11.** Tensile toughness of PHBV/CNW nanocomposite with various CNW contents.

[9,15,44,45]. However, the cold crystallization temperature ($T_{cc}$) progressively decreased with the addition of CNW. This behavior resulted because the CNW is an effective PHBV nucleation agent, which reduced the energy barrier to form PHBV nuclei. Higher contents of CNW induced bigger $T_{cc}$ drop due to larger nucleus-promoting surface provided by CNW. Neat PHBV and all the composites exhibited two melting peaks ($T_{m1}$ and $T_{m2}$), demonstrating a melting-recrystallization-melting process. PHBV crystals with low perfection/low lamella thickness melted at low temperature and subsequently recrystallize to higher perfection, which eventually melted at high temperature.

In the first heating scan no glass transition and cold crystallization could be observed (Fig. 7b) because all the samples were fully crystallized from the long casting process at 50 °C, which is close to PHBV's cold crystallization temperature. Furthermore, $T_{m1}$ and $T_{m2}$ of all the samples measured from the first heating scan were remarkably higher than those measured from the second heating scan. $T_{m1}$ difference between the first and the second scan was ca. 10 °C and the difference for $T_{m2}$ was ca. 7 °C. This indicated that the casting process facilitated PHBV spherulite growth and led to larger lamellar thickness of the spherulites, which consequently exhibited increased melting points. It should be pointed out that no melting of PEG (ca. 66 °C) was detected in both scans. This result might be due to its small concentration (maximum < 2 wt.%) in the composites and its miscibility with PHBV.

The nucleation effect of CNW on PHBV was also investigated by direct POM observation. PHBV spherulites with characteristic banding and Maltese cross could be clearly seen under POM (Fig. 8b). Without CNW powder, the number of PHBV spherulites was small and their size was relatively big because the spherulites had large space to grow before impinging on each other (Fig. 8a,b). With the addition of CNW powder, the number of PHBV spherulites increased significantly and consequently their size was dramatically reduced (see Fig. 8a, c, e for 5 min crystallization and Fig. 8b, d, f for 20 min crystallization). Interpretation of the POM results given clearly suggested the strong nucleation effect of CNW, which was in agreement with DSC findings. Since the CNW powder contained approximately 30 wt.% PEG, its influence on PHBV crystallization was also examined by POM. Fig. 8 g and h showed that 2 wt.% PEG might slightly promote the crystallization of PHBV because more spherulites are evident in the micrographs compared to the neat PHBV. This might be due to the increased mobility of PHBV molecules in the presence of miscible PEG [46].

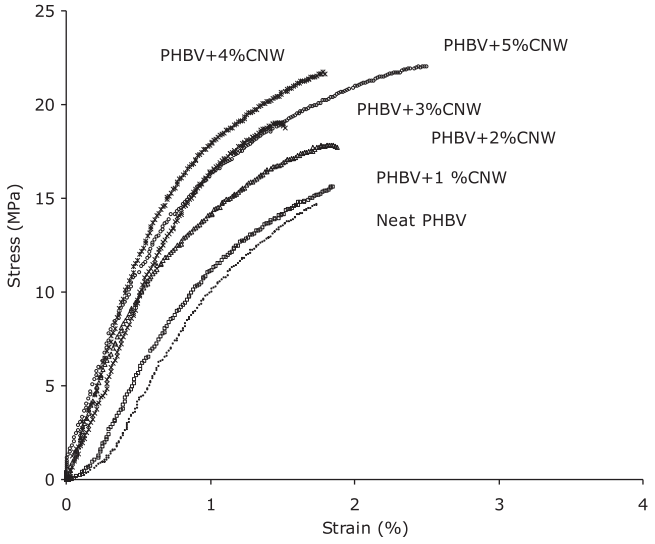


**Fig. 10.** Stress – strain curves of neat PHBV and PHBV/CNW nanocomposites.

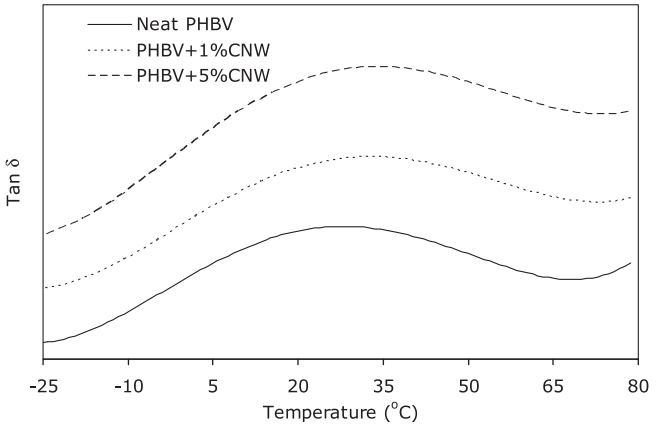


**Fig. 12.** Tan $\delta$ peaks for neat PHBV and PHBV/CNW nanocomposites determined by DMA.

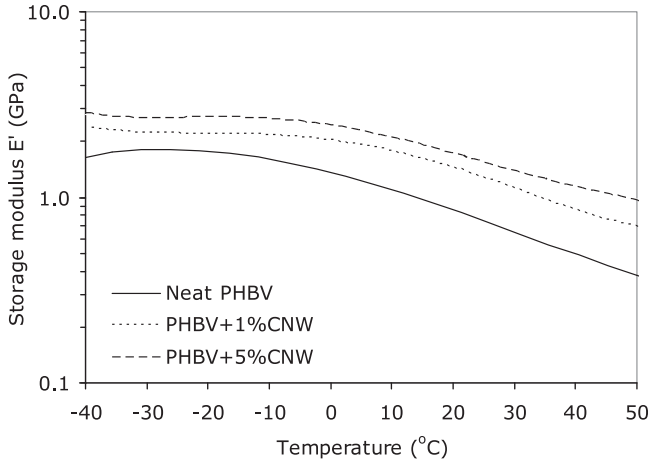


**Fig. 13.** Dependence of the storage modulus on temperature for neat PHBV and PHBV/CNW nanocomposites.

However, it was quite evident that the density of the spherulites with PEG was significantly lower than that with CNW, indicating CNW exhibited much stronger nucleation effect than did PEG. This also suggested that the decrease in $T_{cc}$ observed in DSC tests was mostly caused by the nucleation effect of CNW rather than PEG. Moreover, the nucleation effect of CNW was also compared to that of boron nitride (BN), a commonly used nucleation agent for various polymers. As shown in Fig. 8i and j, PHBV spherulites were nucleated on the BN surface and grew around BN particles (bright spots). Comparing Fig. 8c and d to i and j, it was obvious that CNW induced significantly higher density of PHBV spherulites, indicating that CNW showed stronger nucleation effect compared to the commonly used boron nitride.

### 3.3. Mechanical properties

Mechanical properties of the film samples were examined by both tensile and bulge tests. Young's moduli determined by these two different methods agreed reasonably well (Fig. 9). Indeed, Edwards et al. has shown that tensile and bulge test results complement each other, as bulge test being a perfect tool to measure residual stresses while tensile test for the characterization of linear and nonlinear behavior [47]. Compared to neat PHBV, the moduli of the nanocomposite with 5% CNW powder were increased by 77% (tensile test) and 91% (bulge test), respectively. This modulus increase could be attributed to the restrained chain movement during the deformation due to the existence of CNW. In addition, the refined crystalline structure of the PHBV after the addition of CNW could also influence the modulus of the composites [48–51]. However, the effect varied depending on different polymer systems. Jiang et al. showed that boron nitride refined the crystalline structure of PHBV and decreased the modulus of the PHBV [52]. The tensile strength of the PHBV/CNW composites also increased with the CNW content, indicating strong interfacial bonding between nanoparticles and polymer (Fig. 9). The tensile strength of PHBV/5% CNW was enhanced by 35.5% compared to that of the neat PHBV. Moreover, the tensile toughness, defined as the area below the stress-strain curves (Fig. 10), was also shown to follow the same ascending trend. Toughness increased up to 41% for nanocomposite with the 5 wt.% of CNW powder (Fig. 11).

The effects of CNW on the dynamic mechanical properties of the nanocomposites were examined by DMA. Tan δ of the samples was shown in Fig. 12 (curves are shifted along *y*-axis) and it demonstrated α-relaxations of the samples. Tan δ peak (α-relaxation) was shifted to higher temperatures with the increasing content of CNW powder from 23.8 (neat) to 25.1 (1 wt.% CNW) and 35.2 °C (5 wt.% CNW powder loadings). Moreover, the breadth of the peaks was increased and the intensity of the peaks (damping) was reduced at high CNW contents. Since at temperatures above the Tg, PHBV chains in the amorphous areas of the samples were allowed for long-range cooperative motion, higher transition temperatures indicate that increased energy is required for the chains to perform the motion. This change in energy requirement is likely due to the restraint of CNW and the PHBV spherulites, whose size decreased significantly after the addition of CNW. Peak broadening and reduced damping implied a heterogeneous state of the polymer chains, with the ones in the vicinity of CNW being more restrained and the ones further away being less restrained (or not restrained at all).

Fig. 13 showed that storage modulus of the samples increased with the content of CNW powder. The increase was more significant at the temperatures above the α-relaxation temperatures of the samples. This was because above the transition temperature the modulus of the sample significantly decreased due to the cooperative chain motion. CNW, through its interaction with the chains, restrained the motion of the polymer and therefore to large degree recovered the modulus.

## 4. Conclusions

PHBV/CNW nanocomposites were fabricated by solution casting technique. Morphological study using TEM and AFM revealed good dispersion of CNW in the composites. TGA results demonstrated that the CNW powder contained approximately 30% PEG as a compatibilizer for CNW and the PHBV matrix. Nucleation effect of CNW was confirmed by both DSC and POM. Mechanical properties of the cast films were examined by both tensile and bulge tests and the results from the two tests were in reasonable agreement. With 5 wt.% of CNW, the film showed 77% (by tensile test) and 91% (by bulge test) improvement in Young's modulus, and 35.5% increase in tensile strength. DMA test results demonstrated a 41% increase in storage modulus (at room temperature) and a shift of Tan δ peak to higher temperatures due to CNW's restraint on molecular mobility. Mechanical and dynamic mechanical results indicated that CNW was an effective reinforcing agent for PHBV.

## Acknowledgments

The authors thank National Science Foundation REU program for partial financial support (DMR-0755055).

## References

[1] Ballard D, Holmes P, Senior P. NATO ASI Series, Series C: Math Phys Sci; 1987:293–314.
[2] Pirrotta KMS. Thesis. Princeton University; 1993.
[3] Bauer H, Owen A. Colloid Polym Sci 1988;266:241–7.
[4] Gatenholm P, Kubat J, Mathiasson A. J Appl Polym Sci 1992;45:1667–77.
[5] Mitomo H, Barham P, Keller A. Polym J 1987;19:1241–53.
[6] Avella M, Martuscelli E, Raimo M. J. Mater Sci 2000;35:523–45.
[7] Bondeson D, Mathew A, Oksman K. Cellulose 2006;13:171–80.
[8] Stucova A, Davies G, Eichhorn S. Biomacromolecules 2005;6:1055–61.
[9] Azizi Samir M, Alloin F, Sanchez J, Dufresne A. Polymer 2004;45:4149–57.
[10] Chazeau L, Cavaillé JY, Ganova G, Dendievel R, Boutherin B. J Appl Polym Sci 1999;71:1797–808.
[11] de Rodriguez N, Thielemans W, Dufresne A. Cellulose 2006;13:261–70.
[12] Ljungberg N, Bonini C, Bortolussi F, Boisson C, Heux L, Cavaille JY. Macromolecules 2005;6:2732–9.
[13] Ljungberg N, Cavaillé JY, Heux L. Polymer 2006;47:6285–92.
[14] Helbert W, Cavaillé JY, Dufresne A. Polym Compos 1996;17:604–11.
[15] Hajji P, Cavaillé JY, Favier V, Gauthier C, Vigier' G. Polym Compos 1996;4:612–9.
[16] Ruiz M, Cavaillé JY, Dufresne A, Gerard JF, Graillat C. Compos Interfac 2000;7:117–31.
[17] Ruiz M, Cavaille JY, Dufresne A, Granillat C, Gerard J. Macromol Symp 2001;169:211–22.
[18] Cao X, Dong H, Li C. Biomacromolecules 2007;8:899–904.

[19] Siqueira G, Bras J, Dufresne A. Biomacromolecules 2009;10:425–32.
[20] Dufresne A, Kellerhals M, Witholt B. Macromolecules 1999;32:7396–401.
[21] Anglès M, Dufresne A. Macromolecules 2001;34:2921–31.
[22] Mathew A, Dufresne A. Biomacromolecules 2002;3:609–17.
[23] Kvien I, Sugiyama J, Votrubec M, Oksman K. J Mater Sci 2007;42:8163–71.
[24] Chen Y, Liu C, Chang P, Cao X, Anderson D. Carbohydr Polym 2009;76:607–15.
[25] Qi H, Cai J, Zhang L, Kuga S. Biomacromolecules; 2009.
[26] Wang Y, Cao X, Zhang L. Macromol Biosci 2006;6:524–31.
[27] Mathew A, Oksman K, Sain M. J Appl Polym Sci 2005;97:2014–25.
[28] Oksman K, Mathew A, Bondeson D, Kvien I. Compos Sci Tech 2006;66:2776–84.
[29] Bondeson D, Oksman K. Composites Part A 2007;38:2486–92.
[30] Petersson L, Mathew AP, Oksman K. J Appl Polym Sci 2009;112:2001–9.
[31] Grunert M, Winter WT. J Polym Environ 2002;10:27–30.
[32] Petersson L, Oksman K. Abstracts of Papers, 229th ACS National Meeting, San Diego, CA, United States, March 13-17; 2005.
[33] Goetz L, Mathew A, Oksman K, Gatenholm P, Ragauskas A. Carbohydr Polym 2009;75:85–9.
[34] Braun B, Dorgan J. Biomacromolecules 2009;10:334–41.
[35] Capadona J, Shanmuganathan K, Trittschuh S, Seidel S, Rowan S, Weder C. Biomacromolecules 2009;10:712–6.
[36] Rusli R, Eichhorn S. Appl Phys Lett; 2008:93. 033111/1-033111/3.
[37] Jiang L, Morelius E, Zhang J, Wolcott M, Holbery J. J Compos Mater 2008;42:2629–45.
[38] Di Lorenzo M, Sajkiewicz P, Gradys A, La Pietra P. e-Polymers 2009;(027).
[39] Small M, Nix WJ. Mater Res 1992;7:1553–63.
[40] Kvien I, Tanem BS, Oksman K. Biomacromolecules 2005;6:3160–5.
[41] Avella M, Martuscelli E. Polymer 1988;29:1731–7.
[42] Lu P, Hsieh Y. Nanotechnology 2009;20:415604.
[43] Shimazaki Y, Miyazaki Y, Takezawa Y, Nogi M, Abe K, Ifuku S, et al. Biomacromolecules 2007;8:2976–8.
[44] Favier V, Canova GR, Cavaillé JY, Chanzy H, Dufresne A, Gauthier C. Polym Adv Technol 1995;6:351–5.
[45] Anglè`s M, Dufresne A. Macromolecules 2000;33:8344–53.
[46] You LW, Chiua HJ, Don TM. Polymer 2003;44:4355–62.
[47] Edwards R, Coles G, Sharpe W. Exp Mech 2004;44:49–54.
[48] Supaphol P, Charoenphol P, Junkasem J. Macromol Mater Eng 2004;289:818–27.
[49] Wang J, Qiang D. Polym Int 2008;57:233–9.
[50] Li H, Huneault MA. Polym 2007;48:6855–66.
[51] Tu Z, Mai K, Wu Z. J Appl Polym Sci 2006;101:3915–9.
[52] Jiang L, Huang J, Qian J, Chen F, Zhang J, Wolcott M, et al. J Polym Environ 2008;16:83–93.